Temperature and impurity transport studies of heated tokamak plasmas by means of a collisional-radiative model of x-ray emission from Mo^{30+} to Mo^{39+}

D. Pacella,[1] K. B. Fournier,[1,2] M. Zerbini,[1] M. Finkenthal,[1,3] M. Mattioli,[1] M. J. May,[1,3] and W. H. Goldstein[1,2]
[1]*Associazione EURATOM–ENEA sulla Fusione, 00044 Frascati, Rome, Italy*
[2]*Lawrence Livermore National Laboratory, P.O. Box 808, L-41, Livermore, California 94550*
[3]*Applied Physics Laboratory, The Johns Hopkins University, Johns Hopkins Road, Laurel, Maryland 20723*
(Received 17 June 1999)

This work presents and interprets, by means of detailed atomic calculations, observations of *L*-shell ($n=3\rightarrow n=2$) transitions in highly ionized molybdenum, the main intrinsic heavy impurity in the Frascati tokamak upgrade plasmas. These hot plasmas were obtained by additional electron cyclotron resonance heating (ECRH), at the frequency of 140 Ghz, during the current ramp-up phase of the discharge. Injecting 400 kW on axis and 800 kW slightly off axis, the peak central electron temperature reached 8.0 and 7.0 keV, respectively, for a time much longer than the ionization equilibrium time of the molybdenum ions. X-ray emissions from rarely observed high charge states, Mo^{30+} to Mo^{39+}, have been studied with moderate spectral resolution ($\lambda/\Delta\lambda\sim 150$) and a time resolution of 5 ms. A sophisticated collisional-radiative model for the study of molybdenum ions in plasmas with electron temperature in the range 4–20 keV is presented. The sensitivity of the x-ray emission to the temperature and to impurity transport processes is discussed. This model has been then used to investigate two different plasma scenarios. In the first regime the ECRH heating occurs on axis during the current ramp up phase, when the magnetic shear is evolving from negative to zero up to the half radius. The spectrum is well reproduced with the molybdenum ions in coronal equilibrium and with a central impurity peaking. In the second regime, at the beginning of the current flat top when magnetic shear is monotonic and sawtoothing activity is appearing, the lowest charge states (Mo^{33+} to Mo^{30+}), populated off axis, are affected by anomalous transport and the total molybdenum profile is found to be flat up to the half radius. We conclude with the presentation of ''synthetic spectra'' computed for even higher temperature plasmas that are expected in future experiments with higher ECRH power input.

PACS number(s): 52.55.Fa

I. INTRODUCTION

Progress in magnetic confinement fusion research has produced plasmas with continuously higher temperatures. Moreover, interest in advanced tokamak scenarios is continuously growing, requiring more refined diagnostic tools to investigate particle transport processes. All this has stimulated the study of the atomic physics of highly ionized medium *Z* elements, like molybdenum ($Z=42$). On one hand, the tokamak plasma provides a ''laboratory'' where atomic calculations, relevant in many others fields, can be experimentally validated and, on the other hand, these models allow the understanding of many plasma processes.

In this context a collisional radiative model for the *L*-shell transitions in Mo^{30+} to Mo^{39+} in high temperature plasmas has been developed; details will be presented below. Further, these results have been used to understand the molybdenum x-ray emission from the Frascati tokamak upgrade (FTU) plasma in two different scenarios with electron cyclotron resonance heating (ECRH), providing important information about the plasma impurity content. In the first case, with on axis heating and a central electron temperature T_e of 8 keV, the analysis is performed during the current ramp up when the magnetic shear is still negative or zero [1]. In a toroidal configuration with nested magnetic surfaces, the magnetic shear *s* is a measure of the radial variation of the safety factor *q*, i.e., of the field lines winding index. The magnetic shear is defined by $s=(1/r)dq/dr$ so that shear reversal (i.e., negative shear in the plasma core) implies the presence of an off-axis minimum in the *q* profile. In the second case, with slightly off axis heating and a peak temperature of 7 keV, spectra are analyzed when the current reaches the plateau and sawtooth activity occurs (monotonic *q* profile). These results will be discussed and compared in the following sections.

It must be pointed out that we observe higher ionization degree in molybdenum than previously observed at Alcator C-Mod [2–6] and FTU [7] (the Ne I–like ion and satellites). Be I–and Li I–like Mo line emission has been observed in JET [8] but in a longer wavelength (VUV) range and without any supporting modeling.

The ions of the present work (Mo^{30+} to Mo^{39+}) extend over a large part of the plasma's minor radius ($a=30$ cm) $0<r/a<0.7$. The heating occurs for a time much longer than the ionization equilibrium time τ for these ions in these plasma conditions (the shortest is 1 ms for Mo^{32+} for $T_e=3-5$ keV and the longest is 5 ms for Mo^{38+} for $T_e=6-8$ keV). That is the reason why the study of these spectra, recorded with a time resolution of 5 ms, is a powerful tool to assess the impurity distribution. Finally, the relevance of these ions as diagnostics will be discussed for higher temperature plasmas that will be obtained in future experiments.

II. EXPERIMENTAL CONDITIONS

The two plasma scenarios contrasted in the present work are from discharges where the current reaches its steady state value $I_p=0.7$ MA at $t=0.130$ s. In Ref. [9] the characteristics and the performance of the FTU tokamak are discussed.

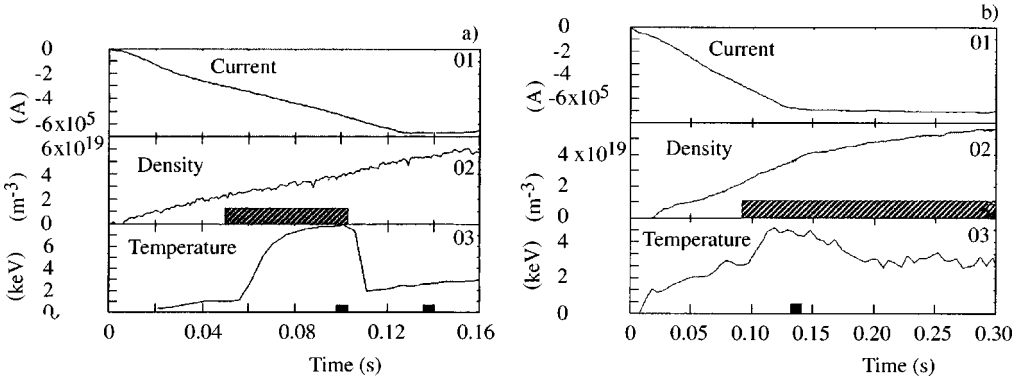

FIG. 1. Time history, during the start-up phase, of the plasma current (top), electron density (middle), and central electron temperature (bottom) for shots 12 658 (a) and 15 505 (b). In the shadowed area the time interval of the ECRH heating is shown. Black boxes indicate the times of the soft-x-ray spectra.

In the first case [Fig. 1(a)], shot 12 658, ($B_t = 5.4$ T) ECRH heating takes place on axis, and the spectrum is analyzed at $t = 0.1$ s when $N_e = 0.4 \times 10^{20}\,\mathrm{m}^{-3}$. In the second case, shot 15 505, ($B_t = 5.7$ T) ECRH heating is injected off axis, the spectrum is studied at $t = 0.135$ s when $N_e = 0.4 \times 10^{20}\,\mathrm{m}^{-3}$ and sawtooth activity started at $t = 0.070$ s. Electron cyclotron waves at 140 GHz, corresponding to a resonant magnetic field of 5 T in the first harmonic, are injected into the plasma. The total ECRH power is 400 (shot 12 658) and 800 kW (shot 15 505) [10]. The launch is perpendicular, from the low field side, with ordinary polarization. The cutoff density, at 140 GHz, is $2.4 \times 10^{20}\,\mathrm{m}^{-3}$, is well above the plasma density. The time history of the plasma current, density central electron temperature, and ECRH pulse are shown in Figs. 1(a) (shot 12 658) and 1(b) (shot 15 505).

For this paper, the plasma electron temperature has been measured by electron cyclotron emission (ECE) with a Michelson interferometer, with 5 ms time resolution and spectral range extending up to 1300 GHz [11]. The spatial resolution is 2 cm in both radial and vertical directions. In Fig. 2 the radial profiles of the electron temperature (T_e) are shown for both discharges, as measured by ECE. In order to evaluate the suprathermal effects during the ECRH, the expected ECE spectrum has been calculated by means of a three-dimensional (3D) bounce-averaged Fokker-Planck code, using the experimental density, temperature and the measured characteristics of the EC wave beam [12]. The wave propagation is computed by means of a toroidal ray-tracing code. The measured ECE spectrum shows a clear separation between the harmonics (Fig. 3), in good agreement with the calculated spectrum, showing that even at these low plasma densities and high temperatures the suprathermal effects are negligible.

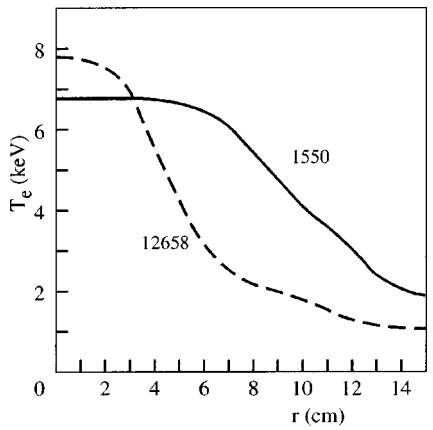

FIG. 2. Electron temperature profile, measured from ECE, at the time $t = 0.1$ s (shot 12 658) and $t = 0.135$ s (No. 15 505).

III. SOFT-X-RAY SPECTRA

The x-ray spectra in the present work were recorded with a spectrometer that uses a simple Bragg configuration with a rotating crystal and an extended Multiwire Proportional Chambers (MWPC) detector that allows discrimination of the different orders of diffraction by exploiting the different detection efficiency in each chamber [13]. The resolving power $\lambda/\Delta\lambda$, ranging from 200 at 5.6 Å to 20 at 0.5 Å, is approximately 150 in the region of the Mo emission.

A spectrum recorded across the entire energy range of the crystal is shown in Fig. 4. The high energy features (~1.2–2.6 Å) are the K_α transitions of ions of Ni, Fe, Mn, Cr, and Ti; the lower energy features (~3.9–5.6 Å) are the *L*-shell transitions ($n = 3 \rightarrow n = 2$) in Mo^{30+} to Mo^{39+}. The discontinuity at 3.89 Å is due to the *K* absorbing edge of the gas (Ar)

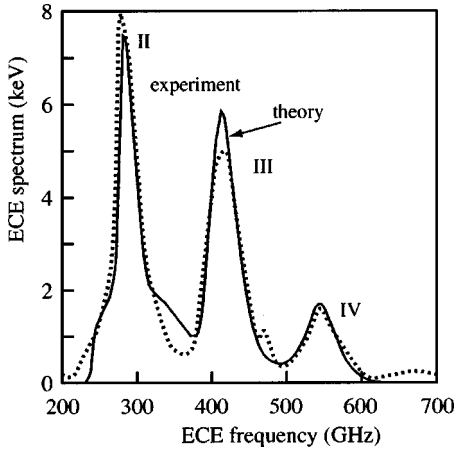

FIG. 3. Electron temperature spectrum measured from ECE (dashed line) compared with the calculated one (continuous line) in the case of no suprathermal electron population. The ECE harmonic numbers are shown.

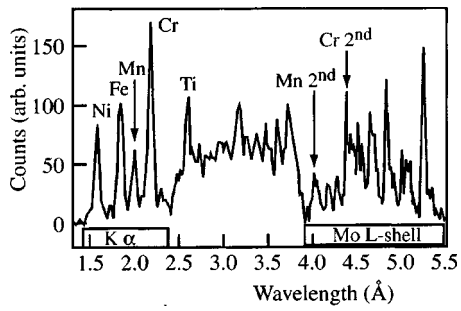

FIG. 4. Full range soft-x-ray spectrum acquired with a rotating crystal spectrometer (shot 12 658). Mo emission falls in the range 3.9–5.4 Å together with the second order of Mn and Cr $K\alpha$ lines.

in the MWPC detector. The second order of diffraction of the Mn and Cr $K\alpha$ features falls in the spectral region of the molybdenum emissions for shot 12 658. Their two contributions have been assessed and subtracted from the molybdenum spectrum.

Two molybdenum spectra from shot 12 658, one during ECRH and one after, are compared in Fig. 5 (the recording times are marked in Fig. 1). Since the wavelengths are scanned in ≈5 ms, a time shorter than the time evolution of the density and temperature from the point of view of their influence on the spectra under investigation, the plasma can be assumed stationary on this time scale. It is seen that the three features that we label α, β, and γ which are dominated by transitions from Mo^{35+}, Mo^{36+}, and Mo^{37+}, respectively, decrease strongly when the temperature drops, while the remaining spectrum (dominated by Mo^{32+} transitions [7]) is less affected. The detailed modeling of these transitions is discussed below.

IV. COLLISIONAL RADIATIVE MODEL

The methods used to construct the collisional-radiative models of the present work are described in our previous work [7]. In brief, *ab initio* energy levels and radiative transition probabilities have been generated for each ion using the relativistic parametric potential code RELAC [14]. The electron impact excitation rates between all levels in each ion are calculated in the distorted wave approximation using the CROSS code [15]. For Mo^{32+}, the collisional excitation rates have been augmented by the resonant excitation calculations from Chen [16]. Impact ionization from each energy level in

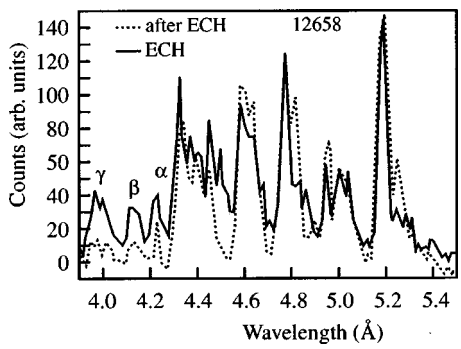

FIG. 5. Comparison of Mo spectrum, during (solid line, $t=0.100-0.105$ s) and after (dotted line, $t=0.135-0.140$ s) ECRH heating (shot 12 658).

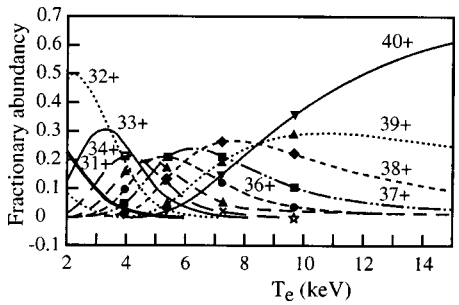

FIG. 6. Ionization equilibrium distribution of Mo ions in the electron temperature range 2–15 keV.

each ion to all possible levels in the next ion have been computed using RELAC's level energies and a modified Lotz formula [17]. For Mo^{31+} and Mo^{30+}, autoionization rates for all inner shell excited levels in the continuum have been computed using RELAC [18]. The molybdenum ionization state distribution has been computed and the fractional abundance curves versus temperature between 2 and 15 keV are shown in Fig. 6. As in our previous work [7], the ground state ionization fractions at a given temperature are held fixed, and the collisional-radiative populations in the excited levels of each ion are then found by solving the set of equations

$$\frac{dn_j}{dt}=\sum_i n_i R_{i\to j}-n_j\sum_i R_{j\to i},$$

where n_i is the population in level i of a given ion, and $R_{i\to j}$ is the rate at which population leaves level i and goes to some level j, possibly belonging to a neighboring isosequence. The resulting intensity of a transition from level i to level j is

$$I_{ij}(T_e)=n_i(T_e)A_{ij},$$

where A_{ij} is the radiative transition rate.

The calculated energies of the levels of the ground state configuration, and some nearby levels, in each molybdenum ion are listed in Table I. The accuracy of the predictions have been confirmed by comparison of x-ray emission from higher n transitions ($n>3\to n=2$) in ions around Ne-like Mo^{32+} observed with high spectral ($\lambda/\Delta\lambda\approx 4000$) resolution in the Alcator *C*-Mod tokamak plasma [2]. The transitions included in the (blended) features marked α, β, and γ (in Fig. 5) are identified in Table II. The collisional-radiative intensity for the components of each feature is also listed for a temperature near which that feature is seen to be dominant.

High resolution synthetic spectra computed for $T_e=3.8$, 5.5, and 8.0 keV are shown in Fig. 7; it should be noted that even if Gaussian shapes with a full width at half maximum (FWHM) of 1.0 mÅ are assumed, blending still persists. As can be seen, the spectra are sensitive to the temperature, both because of changing ionization state distribution (Fig. 6) and, to a lesser extent, because of the temperature dependence of the intensity of individual lines. Each ion (from Mo^{30+} to Mo^{39+}) carries information from the radial layer where it exists; studying these x-ray spectra we obtain spatial information over a large fraction of the minor radius [$0<r/a<0.7$ and $T_e(0)=1-8$ keV]. In particular, the features la-

TABLE I. Electron configurations of low-lying energy levels in Ne I– to Li I–like Mo ions. Each level is indicated by the occupancy of jj-coupling orbitals, where ''+'' indicates $l+s$ coupling and $l+s$ coupling and ''−'' indicates $l-s$ coupling and the total angular momentum J for the level. The calculated level energy (in eV) is referred to the ground state (index 1). The ionization potential is also given.

Index	Orbital occupancies	Total J	Energy
	Ne like, $V_{\text{ion}}=4256.0$ eV		
1	$(2s)^2(2p-)^2(2p+)^4$	0	0.0
	F like, $V_{\text{ion}}=4426.9$ eV		
1	$(2s)^2(2p-)^2(2p+)^3$	3/2	0.0
2	$(2s)^2(2p-)^1(2p+)^4$	1/2	109.76
3	$(2s)^1(2p-)^2(2p+)^4$	1/2	331.11
	O like, $V_{\text{ion}}=4602.2$ eV		
1	$(2s)^2(2p-)^2(2p+)^2$	2	0.0
2	$(2s)^2(2p-)^2(2p+)^2$	0	27.48
3	$(2s)^2(2p-)^1(2p+)^3$	1	105.78
4	$(2s)^2(2p-)^1(2p+)^3$	2	121.30
5	$(2s)^2(2p+)^4$	0	241.14
	N like, $V_{\text{ion}}=4779.1$ eV		
1	$(2s)^2(2p-)^2(2p+)^1$	3/2	0.0
2	$(2s)^2(2p-)^1(2p+)^2$	3/2	96.28
3	$(2s)^2(2p-)^1(2p+)^2$	5/2	113.91
4	$(2s)^2(2p-)^1(2p+)^2$	1/2	136.61
5	$(2s)^2(2p+)^3$	3/2	236.23
	C like, $V_{\text{ion}}=5081.8$ eV		
1	$(2s)^2(2p-)^2$	0	0.0
2	$(2s)^2(2p-)^1(2p+)^1$	1	101.02
3	$(2s)^2(2p-)^1(2p+)^1$	2	114.97
4	$(2s)^1(2p-)^2(2p+)^1$	2	226.51
5	$(2s)^2(2p+)^2$	2	228.09
6	$(2s)^2(2p+)^2$	0	260.29
	B like, $V_{\text{ion}}=5266.3$ eV		
1	$(2s)^2(2p-)^1$	1/2	0.0
2	$(2s)^1(2p-)^2$	1/2	107.03
3	$(2s)^2(2p+)^1$	3/2	121.20
4	$(2s)^1(2p-)^1(2p+)^1$	3/2	193.75
5	$(2s)^1(2p-)^1(2p+)^1$	7/2	219.11
6	$(2s)^1(2p-)^1(2p+)^1$	3/2	257.94
7	$(2s)^1(2p-)^1(2p+)^1$	1/2	262.64
	Be like, $V_{\text{ion}}=5550.4$ eV		
1	$(2s)^2$	0	0.0
2	$(2s)^1(2p-)^1$	0	74.89
3	$(2s)^1(2p-)^1$	1	90.57
4	$(2s)^1(2p+)^1$	2	198.17
5	$(2p-)^2$	0	218.00
6	$(2s)^1(2p+)^1$	1	249.77
	Li like, $V_{\text{ion}}=5713.2$ eV		
1	$(2s)^1$	1/2	0.0
2	$(2p-)^1$	1/2	86.520
3	$(2p+)^1$	3/2	212.32

beled α, β, and γ are typical of the higher temperature regime ($T_e>3$ keV) and drop in intensity when the ECRH is switched off (Fig. 5); γ is dominated by B-like Mo^{37+} which exists in appreciable amounts only in plasmas with $T_e \geqslant 5$ keV (see Fig. 8), while α, β are dominated by lines from N-like Mo^{35+} and C-like Mo^{36+}, respectively. The features α, β, and γ depend strongly on the electron temperature, as can be seen, for example, in Fig. 9 where their brightnesses are calculated for a range of plasmas with a single temperature.

V. SIMULATIONS OF THE SPECTRA AND RESULTS

The collisional-radiative model described above is used to reconstruct the measured molybdenum spectra knowing the

TABLE II. Calculated transitions that comprise the features α, β, γ. The upper level of each transition is indicated by the occupancy of jj-coupling orbitals where ''+'' indicates $l+s$ coupling and ''−'' indicates $l-s$ coupling. Numbers in braces indicate powers of ten, i.e., $X[-Y]=X\times10^{-Y}$. The line intensity is calculated, in units of photons/(s cm^3 $n_e n_{\rm ion}$), using a collisional radiative model for a plasma at temperature $T_e=4$ keV for the feature α, 6 keV for β, and 8 keV for γ. Lines that will make up features at higher temperatures are also listed.

Ion	Transition	CR intensity[a]	Oscillator strength[b]	$\lambda^{\rm calc}$ (Å)
	Feature α at $T_e=4$ keV			
B	$6\leftarrow(2s)^1(2p-)^1(3d+)^1\ J=5/2$	2.40[−12]	1.818[+00]	4.2476
B	$6\leftarrow(2s)^1(2p-)^1(3d+)^1\ J=3/2$	3.58[−13]	2.476[−01]	4.2488
N	$1\leftarrow(2s)^2(2p-)^1(2p+)^1(3d-)^1\ J=1/2$	2.72[−12]	8.723[−01]	4.2502
N	$1\leftarrow(2s)^2(2p-)^1(2p+)^1(3d-)^1\ J=3/2$	3.99[−12]	1.525[−00]	4.2541
B	$7\leftarrow(2s)^1(2p-)^1(3d+)^1\ J=3/2$	1.66[−12]	1.151[+00]	4.2556
N	$1\leftarrow(2s)^2(2p-)^1(2p+)^1(3d-)^1\ J=5/2$	2.86[−12]	1.442[+00]	4.2557
N	$1\leftarrow(2s)^2(2p-)^1(2p+)^1(3d+)^1\ J=5/2$	1.97[−12]	1.027[+00]	4.2699
Ne[c]	$1\leftarrow(2s)^1(2p-)^2(2p+)^4(3d+)^1\ J=2$	2.21[−12]		4.2729
N	$1\leftarrow(2s)^2(2p-)^1(2p+)^1(3d-)^1\ J=5/2$	9.70[−13]	2.881[−01]	4.2892
N	$1\leftarrow(2s)^2(2p-)^1(2p+)^1(3d-)^1\ J=3/2$	6.82[−13]	2.688[−01]	4.2921
C	$2\leftarrow(2s)^2(2p-)^1(3d-)^1\ J=1$	1.51[−12]	1.677[-0^1]	4.2927
F	$1\leftarrow(2s)^1(2p^-)^2(2p^+)^3(3p+)^1\ J=3/2$	3.38[−13]	1.125[−01]	4.2933
F	$1\leftarrow(2s)^1(2p-)^2(2p+)^3(3p+)^1\ J=5/2$	9.83[−13]	3.163[−01]	4.2957
	Feature β at $T_e=6$ keV			
Li	$3\leftarrow(3s+)^1\ J=1/2$	1.33[−12]	7.701[−02]	4.1402
Be	$6\leftarrow(2s)^1(3d+)^1\ J=2$	6.28[−12]	1.931[+00]	4.1420
C	$1\leftarrow(2s)^2(2p-)^1(3d-)^1\ J=1$	1.64[−11]	1.405[+00]	4.1476
C	$3\leftarrow(2s)^2(2p+)^1(3d-)^1\ J=3$	9.29[−13]	2.556[+00]	4.1482
	Feature γ at $T_e=8$ keV			
Li	$3\leftarrow(3d+)^1\ J=5/2$	2.57[−12]	2.443[+00]	4.0308
B	$1\leftarrow(2s)^2(3d-)^1\ J=3/2$	1.07[−11]	1.539[+00]	4.0350
B	$1\leftarrow(2s)^1(2p-)^1(3p-)^1\ J=1/2$	3.92[−13]	6.223[−02]	4.0385
Be	$3\leftarrow(2s)^1(3s+)^1\ J=0$	4.94[−13]	6.293[−03]	4.0560
C	$1\leftarrow(2s)^1(2p-)^2(3p+)^1\ J=1$	3.68[−12]	4.185[−01]	4.0585
	Even shorter λ at $T_e=8$ keV			
Be	$1\leftarrow(2s)^1(3p-)^1\ J=1$	2.20[−12]	1.995[−01]	3.9141
Be	$3\leftarrow(2s)^1(3d-)^1\ J=2$	6.74[−13]	1.474[+00]	3.9580
B	$1\leftarrow(2s)^1(2p-)^1(3p+)^1\ J=3/2$	2.48[−12]	4.468[−01]	3.9609
B	$1\leftarrow(2s)^1(2p-)^1(3p+)^1\ J=1/2$	1.67[−12]	2.987[−01]	3.9629
Li	$1\leftarrow(3p+)^1\ J=3/2$	2.63[−12]	4.722[−01]	3.7936
Li	$1\leftarrow(3p-)^1\ J=1/2$	1.53[−12]	2.610[−01]	3.8375
Be	$1\leftarrow(2s)^1(3p+)^1\ J=1$	5.38[−12]	4.919[−01]	3.8673
Li	$2\leftarrow(3d-)^1\ J=3/2$	1.47[−12]	1.295[+00]	3.8866

[a]CR intensity in units of photons /s cm^3 $n_e n_{\rm ion}$.
[b]Weighted oscillator strength $(2j_{\rm low}+1)f_{\rm low\to up}$.
[c]$E2$ (electric quadrupole) transition.

electron temperature and density profiles. This is possible since the typical times τ required for these ions to reach ionization equilibrium in this temperature and density range are a few milliseconds. Since the central electron temperature reaches nearly its peak value 20 ms (Δt) before the spectrum in Fig. 5 is recorded ($t\cong0.1$ s), the ions have enough time ($\Delta t\gg\tau$) to reach the equilibrium.

The brightness B (photons/s cm^2 sr) of features in the wavelength range $\lambda_1-\lambda_2$ can be calculated by means of the following integral:

$$B=\frac{1}{2\pi}\int_0^a dr\,N_e(r)N_{\rm Mo}(r)\int_{\lambda_1}^{\lambda_2}d\lambda\sum_Z\ \mathcal{E}_Z(\lambda,T_e(r))f_Z(r),$$

where r is the radial coordinate of the circular cross section, ''a'' is the plasma minor radius, f_Z is the fractional abundance of ion Z, N_e is the electron, and $N_{\rm Mo}$ is the total molybdenum radial density profile. The emissivity $\mathcal{E}_Z$(photons/s cm^3N_eN_Z) per unit electron and ion density of ion ''Z'' (Table II) at temperature T_e is calculated from the

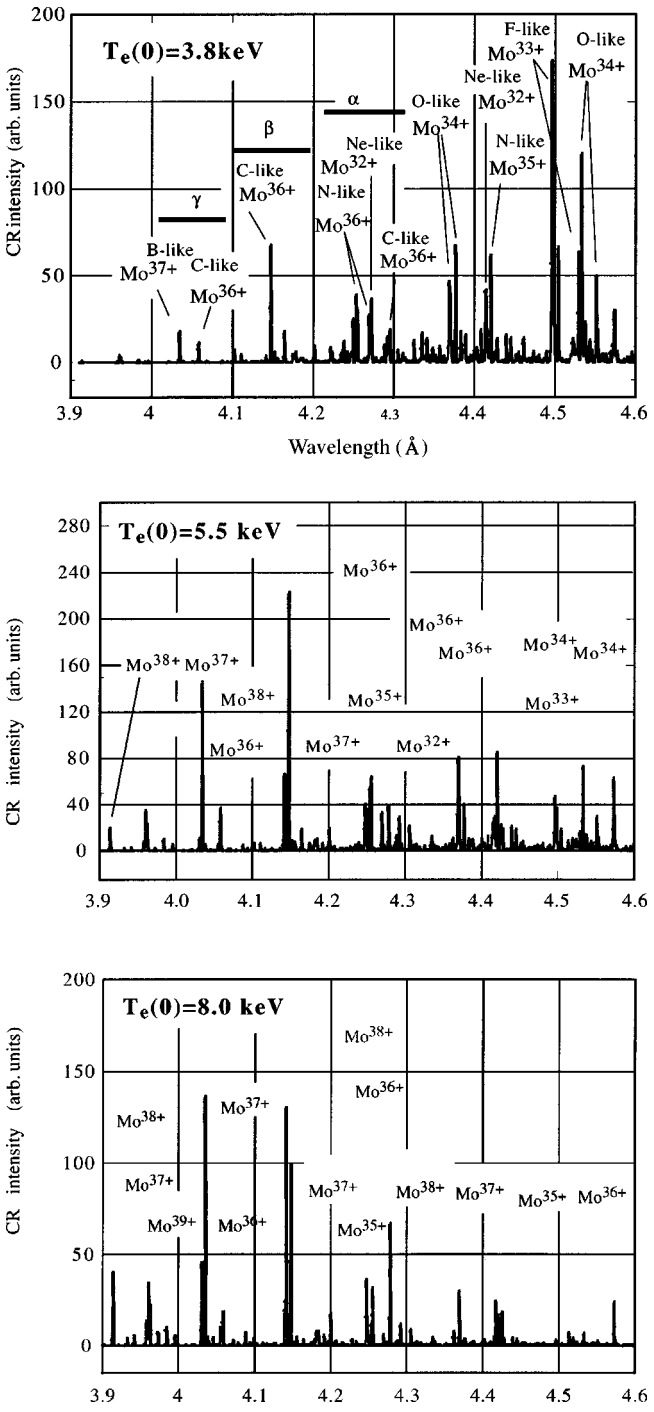

FIG. 7. Calculated spectra, at high resolution, of the Mo highly ionized charge states for a homogeneous plasma with density 10^{20} m^{-3} and temperature, respectively, of 3.8, 5.5, and 8.0 keV.

collisional-radiative model. Theoretical spectra, calculated using these emissivities $\mathcal{E}_Z$, are shown, for three different electron temperatures in Figs. 7 and 8 with high and low spectral resolution, respectively.

In order to simulate the line of sight of the spectrometer the radial coordinate is divided into 18 values, and at each point of the grid all the quantities in the integral in Eq. (3) are calculated. The integration is then done numerically. To simulate the low resolution of the spectrometer, each feature is given a Gaussian shape with a FWHM of 0.04 Å (corresponding to the resolving power of the spectrometer in this

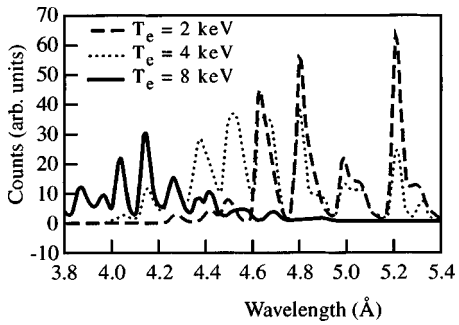

FIG. 8. Calculated spectra, at low resolution, for a homogeneous plasma at electron temperature of 2.0, 4.0, and 8.0 keV.

energy range). The resulting intensity is integrated in wavelength to produce a final, blended spectrum.

$N_{Mo}(r)$ and $f_Z(r)$ are free parameters and the best fit of the experimental spectrum will provide an assessment of these unknown functions. The first step is to simulate the three features α, β, and γ. Since α, β, and γ are emitted in the first 4 cm from the center, the total molybdenum profile $N_{Mo}(r)$ can be assumed flat in this very central region and we can perform the fit considering f_Z the only free parameter. The result is that the experimental spectrum for α, β, and γ [Fig. 10] is well simulated taking the central ions, Mo^{35+} to Mo^{39+}, in coronal equilibrium [Fig. 11(a)] with the electron temperature profile as measured from ECE. These central ions do not show anomalous transport. The feature at 4.75–4.9 Å, emitted by Mo^{32+}, Mo^{31+}, and Mo^{30+} is also well simulated using the coronal equilibrium charge state distribution for these ions. A verification of this result was obtained using an impurity transport code, developed by one of the authors (Mattioli) [19]. Simulations of molybdenum in flow in this plasma ramp up phase have been done with the anomalous transport coefficients commonly used to model the flat top phase of other FTU discharges [20]. The diffusion coefficient D is 0.8 m^2/s and the convective velocity V is 10 m/s, with a peaking parameter $S=1.8$. With these anomalous transport parameters, the ionization equilibrium time is longer than in the coronal equilibrium case, and the changes in the density and temperature profiles in time have to be taken into account. To simulate this dynamic phase

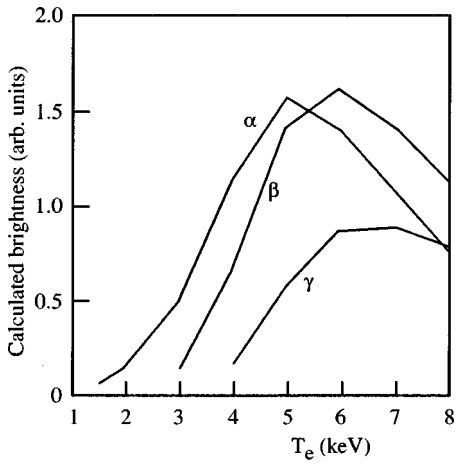

FIG. 9. Calculated brightnesses of the features α,β,γ for a homogeneous plasma at different values of electron temperature.

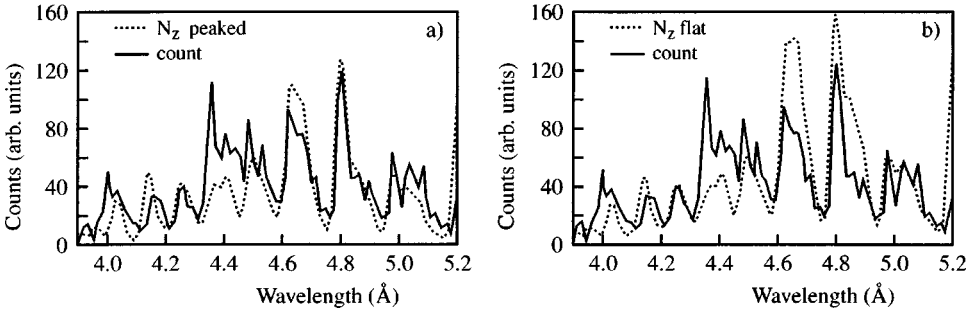

FIG. 10. Comparison between measured (shot 12 658) soft-x-ray Mo spectrum (continuous line) and the simulated one (dashed line) for two cases. (a) Best fit of the experimental spectrum using a central peaked total molybdenum radial profile. (b) The same with a flat total molybdenum radial profile.

(0–100 ms), a few time-dependent simulations were performed for partial time intervals. The ion profiles calculated in the coronal model and those with anomalous transport are compared in Fig. 11 [11(a) and 11(b), respectively]. In the case with anomalous transport, the ionization degree is much lower in the plasma core and all the lines emitted by Mo^{35+} to Mo^{39+} are suppressed, clearly in contrast with what observed.

The second step is to simulate the full spectrum, and in particular the relative ratio of these features (α, β, γ) with respect to the resonant lines at 4.8–4.9 Å from Mo^{32+}, Mo^{31+}, and Mo^{30+}. (These features are better understood than those at 4.5–4.6 Å from Mo^{34+} and Mo^{33+}.) This ratio depends strongly on the total impurity profile $N_{Mo}(r)$. The synthetic and experimental spectra are shown in Fig. 10(a) for a peaked impurity profile and Fig. 10(b) for a flat one (continuous line represents the experimental spectrum). The peaked impurity profile $N_{Mo}(r)$, normalized at its value at $r=15$ cm, is shown in Fig. 12 together with the electron density profile normalized at its central value. The peaked profile gives the best fit of the experimental spectrum. This assessment of the impurity radial density profile is robust because relies on agreement from all the emitting ions (Mo^{39+} to Mo^{30+}), over the whole radial range $0<r/a<0.7$ and not just on the ''high temperature'' features. The calculated feature β is narrower and higher with respect to the measured one, but the integral is the same; this is due to spurious blending of several of the weak lines making up this feature.

These two results, an impurity transport level much lower with respect to that one usually measured at FTU in the steady state and a central impurity peaking, are compatible with a neoclassical transport regime. The central densities of Ni, Fe, Mn, Cr, and Ti have been assessed using the $K\alpha$ emissions measured with the same spectrometer and shown in Fig. 4 and the total central Z_{eff} is found to be around 9. An independent assessment, based on the Spitzer resistivity reproducing the loop voltage, gives $Z_{eff}=6.7$. These values, exceptionally high for FTU plasmas, are due to the low electron density and the central impurity peaking. The result concerning the impurity behavior should be related to the good energy confinement property of the bulk observed in a previous work [1] studying the energy balance and the thermal conduction for the same shot (12 658). The electron thermal diffusivity profile is found to be below 0.4 m^2/s within one-third of the plasma radius, with a minimum of 0.2 m^2/s. It is remarkable that these values close to the lowest ones found in Ohmic discharges have been obtained in the presence of almost an order of magnitude larger fluxes and gradients.

In contradistinction to the case above, a second discharge was studied in a different transport regime. In this shot (15 505) ECRH heating off axis was used with double power (800 kW) on the same plasma target. The Mo emissions were analyzed at a later time ($t=0.135$ s) after the current flat top had been reached and after the onset of the sawtooth insta-

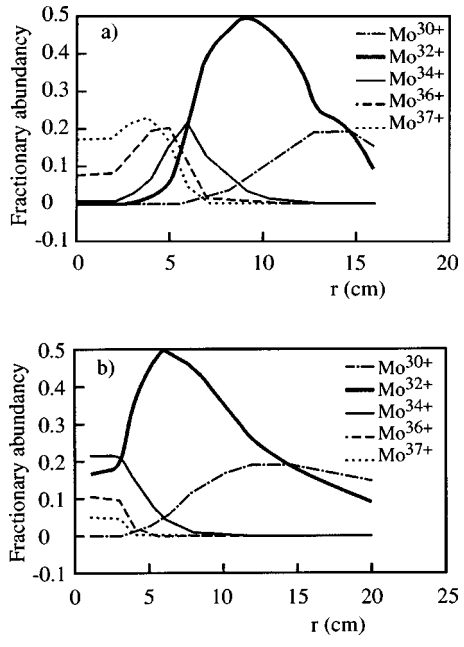

FIG. 11. Fractional abundance curves versus radius for core Mo ions in two cases. (a) No impurity transport (coronal equilibrium). (b) Anomalous transport with diffusion coefficient $D=0.8$ m^2/s and convective velocity $V=10$ m/s.

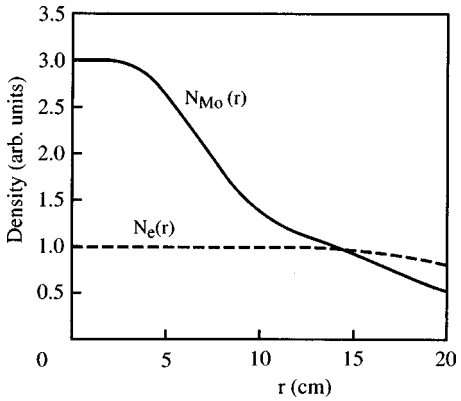

FIG. 12. Central peaked total molybdenum radial profile used in the best fit of Fig. 10(a) together with the electron density profile at $t=0.1$ s (shot 12 658).

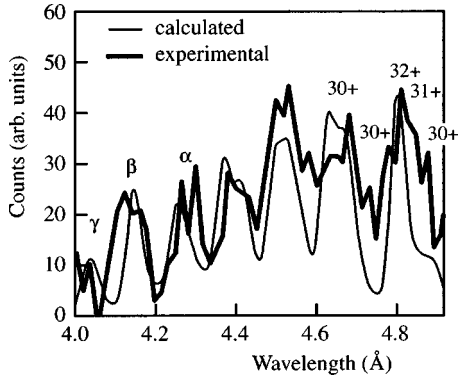

FIG. 13. Best fit (thin line) of the measured soft-x-ray Mo spectrum (thick line) for shot 15 505 ($t=0.135-0.140$ s).

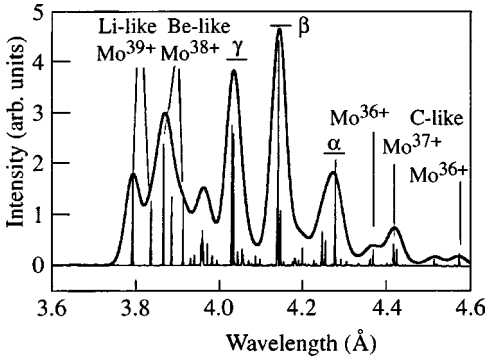

FIG. 14. Simulated spectrum at high resolution ($\lambda/\Delta\lambda=4000$) and convolution at low resolution ($\lambda/\Delta\lambda=200$) (bold line) for the most ionized Mo ions in a plasma at 11 keV.

bility ($t=0.070$ s). The off axis heating (resonance at $r=7$ cm) and the presence of the sawtooth crashes produce a plateau in the central electron temperature (Fig. 2) and a much broader region emitting at high temperature. We have applied the same method to simulate the experimental spectrum (thick line in Fig. 13). The features α, β, and γ are well simulated with the emitting ions (Mo^{35+} to Mo^{39+}) in coronal equilibrium. Further, the relative ratio of these high temperature features with the line of Mo^{32+} at 4.8 Å is well reproduced with a total molybdenum profile $N_{Mo}(r)$ almost flat. However, the features between 4.6 and 4.9 Å are not well simulated with the assumption of coronal equilibrium, in particular the lines emitted by Mo^{31+} and Mo^{30+} are underestimated. This implies that in the radial region where these two ions exist ($r/a>0.3$) anomalous transport is now present, reducing the degree of ionization. Unlike the previous case, in this phase of the discharge the shear has become positive and the anomalous transport appeared, particularly in the half radius region. This observation is in agreement with the results founds in a recent work [21], where molybdenum impurity transport is measured and modeled as driven by electrostatic turbulence [22] during the current flat top phase. In this case the transport of the majority species (deuterium) is typical of the current flat-top phase. In Ohmic discharges with the same current and density, the electron thermal diffusivity is found to be, at half radius, in the range from 0.4 to 0.8 m^2/s [23]. Moreover, global analysis shows that the energy confinement time scales with the total input power as expected for the *L*-mode scaling law.

VI. CONCLUSIONS

A collisional-radiative model of molybdenum x-ray emission from a high temperature plasma has been developed and discussed. It has been used to interpret the spectra recorded on the FTU Tokamak. This method gives relevant information about the impurity behavior in different plasma conditions. In the first case, a spectrum in the current ramp up phase shows that the molybdenum ions are in coronal equilibrium over most of the minor radius ($0<r/a<0.7$) and that they accumulate at the center. In the second case, when the current flat top is approached, the anomalous transport affects the ion distribution and the total molybdenum profile is flattened. The ionization balance is in general sensitive to the distorsion of the distribution function of the electrons. It will be therefore very interesting, in the future, to study the x-ray spectra at lower density, where important distorsions of the electron distribution function due to ECRH heating are expected.

We remark that molybdenum is an excellent diagnostic tool because it has several ions that emit strongly and have appropriate ionization times ($\tau\sim ms$) in the temperature range up to 20 keV. In particular the resonant lines of the B I–, Be–I–, Li I–like ions are bright and can be used as diagnostics of very high temperature plasmas in the same way as the N I–, C I–, and B I–like ions have been used in the present work. A synthetic spectrum for Mo^{37+} to Mo^{40+} both at high and low spectral resolution is shows in Fig. 14 for an electron temperature of 11 keV. The present experiments at FTU were performed with one and two gyrotrons; the installation of four tubes with a total power of 1.6 MW at the plasma is now in progress. Consequently, in future experiments temperatures greatly in excess of 8 keV are expected and other plasma scenarios will be accessible; these ions will provide an excellent diagnostic tool to study these plasmas.

ACKNOWLEDGMENTS

The present work was performed in collaboration with the U.S. Department of Energy by the Lawrence Livermore National Laboratories under Contract No. W-7405-ENG-48. The authors wish to thank the members of the FTU team and ECRH teams, in particular S. Cirant, G. Granucci, A. Bruschi, A. Simonetto, and C. Sozzi.

[1] P. Buratti *et al.*, Phys. Rev. Lett. **82**, 569 (1999).
[2] J. E. Rice, K. B. Fournier, M. A. Graf, J. L. Terry, M. Finkenthal, F. Bombarda, E. S. Marmar, and W. H. Goldstein, Phys. Rev. A **51**, 3551 (1995); J. E. Rice, K. B. Fournier, M. A. Graf, J. L. Terry, M. Finkenthal, E. S. Marmar, and W. H. Goldstein, *ibid.* **53**, 3953 (1996).
[3] J. E. Rice *et al.*, J. Phys. B **29**, 2191 (1996).
[4] J. E. Rice *et al.*, Nucl. Fusion **37**, 421 (1997).
[5] M. J. May *et al.*, Nucl. Fusion **37**, 881 (1997).
[6] J. E. Rice *et al.*, Fusion Eng. Des. **34–35**, 159 (1997).

[7] K. B. Fournier *et al.*, Phys. Rev. E **53**, 1 (1996); **53**, 1084 (1996).
[8] Denne B *et al.*, Phys. Rev. A **40**, 3702 (1989).
[9] R. Andreani, Fusion Eng. Des. **22**, N1–2 (1993); **22**, 129 (1993).
[10] S. Cirant *et al.*, in *Proceedings of the Tenth Joint Workshop on ECE and ECRH, Ameland, The Netherlands, 1997*, edited by T. Donne and T. Verhoeven (World Scientific, Singapore, 1997), p. 369.
[11] P. Buratti and M. Zerbini, Rev. Sci. Instrum. **66**, 4208 (1995).
[12] M. Zerbini *et al.*, Rev. Sci. Instrum. (to be published).
[13] R. Bartiromo *et al.*, Nucl. Instrum. Methods Phys. Res. B **95**, 537 (1995).
[14] M. Klapisch *et al.*, J. Opt. Soc. Am. **67**, 148 (1977).
[15] A. Bar-Shalom, M. Klapisch, and J. Oreg, Phys. Rev. A **38**, 1773 (1988).
[16] M. Chen and K. Reed, Phys. Rev. A **40**, 5 (1989); **40**, 2292 (1989).
[17] W. Lotz, Z. Phys. **232**, 101 (1970).
[18] J. Oreg, W. Goldstein, P. Mandelbaum, D. Mitnik, E. Meroz, J. Schwob, and A. Bar Shalom, Phys. Rev. A **44**, 3 (1991); **44**, 1741 (1991); J. Oreg, W. Goldstein, and M. Klapisch, *ibid.* **44**, 3 (1991); **44**, 1750 (1991).
[19] M. Mattioli, C. DeMichelis, and A. Pecquet, Nucl. Fusion **38**, 1629 (1998).
[20] D. Pacella *et al.* (unpublished).
[21] D. Pacella *et al.* (unpublished).
[22] F. Romanelli and F. Zonca, Phys. Fluids B **5**, 11 (1993).
[23] G. Bracco, P. Buratti, and O. Tudisco (unpublished).